

Article

Three-Dimensional CFD Modeling of Transport Phenomena in a Cross-Flow Anode-Supported Planar SOFC

Zhonggang Zhang ^{1,2}, Jingfeng Chen ², Danting Yue ¹, Guogang Yang ¹, Shuang Ye ³, Changrong He ³, Weiguo Wang ³, Jinliang Yuan ^{4,*}, Naibao Huang ⁵

¹ Marine Engineering College, Dalian Maritime University, Dalian 116026, China; E-Mails: zhgang0530@163.com (Z.Z.); yuedanting@163.com (D.Y.); ygg@dlnu.edu.cn (G.Y.)

² Marine Engineering College, Jimei University, Xiamen 361021, China; E-Mail: jingfengchen@126.com

³ Ningbo Institute of Material Technology and Engineering (NIMTE), Chinese Academy of Science, Ningbo 315201, China; E-Mails: yeshuang@nimte.ac.cn (S.Y.); hechangrong@nimte.ac.cn (C.H.); wgwang@nimte.ac.cn (W.W.)

⁴ Department of Energy Sciences, Lund University, Box 118, 22100 Lund, Sweden

⁵ Transportation Equipment and Ocean Engineering College, Dalian Maritime University, Dalian 116026, China; E-Mail: naibaohuang@gmail.com

* Author to whom correspondence should be addressed; E-Mail: jinliang.yuan@energy.lth.se; Tel.: +46-46-222-4813; Fax: +46-46-222-4717.

Received: 22 November 2013; in revised form: 18 December 2013 / Accepted: 23 December 2013 / Published: 31 December 2013

Abstract: In this study, a three-dimensional computational fluid dynamics (CFD) model is developed for an anode-supported planar SOFC from the Chinese Academy of Science Ningbo Institute of Material Technology and Engineering (NIMTE). The simulation results of the developed model are in good agreement with the experimental data obtained under the same conditions. With the simulation results, the distribution of temperature, flow velocity and the gas concentrations through the cell components and gas channels is presented and discussed. Potential and current density distributions in the cell and overall fuel utilization are also presented. It is also found that the temperature gradients exist along the length of the cell, and the maximum value of the temperature for the cross-flow is at the outlet region of the cell. The distribution of the current density is uneven, and the maximum current density is located at the interfaces between the channels, ribs and the electrodes, the maximum current density result in a large over-potential and heat source in the electrodes, which is harmful to the overall performance and working lifespan of the fuel cells. A new type of flow structure should be developed to make the current flow be

more evenly distributed and promote most of the TPB areas to take part in the electrochemical reactions.

Keywords: simulation; cross-flow; electrochemical reaction; 3D CFD model; transfer phenomena

1. Introduction

Fuel cells can directly convert the free energy of a chemical reactant into electrical energy and heat, which is different from a conventional thermal power plant, where the fuel is oxidized in a combustion process combined with a conversion process (thermal-mechanical-electrical energy), that takes place after the combustion [1]. If pure hydrogen is used, no air or environmental pollution occurs at all, because the output from the fuel cells is electricity, heat and water. High temperature solid oxide fuel cells (SOFCs), with their advantages of high efficiencies, environmental friendliness and flexibility of fuel types that can be used, have been considered as one of the most promising technologies for electricity generation [2].

Depending on the specific configuration and design, a variety of physical phenomena are present in an SOFC, e.g., multi-component gas flow, energy and mass transfer of chemical species in composite domains, even at the micro- and nano-scale levels. Due to the electrochemical reactions, generation and consumption of chemical species together with current production are involved at the active surfaces in SOFCs. All these are inaccessible to experimental measurements, so computational fluid dynamics (CFD) methods are becoming more attractive.

The aim of the study presented in this paper is to investigate the transport phenomena inside an single SOFC fed with hydrogen as the fuel and to evaluate its overall performance. For this purpose a three-dimensional CFD model has been developed for an anode-supported planar SOFC. With the modeling results, the distribution of temperature, flow velocity, the gas concentrations (fuel and air) through the cell structure and gas channels is discussed. Electric potential and current density distributions over the cell and fuel utilization are also computed. The commercial CFD code Ansys FLUENT is used to solve the mass, momentum, energy and charge conservation. The electrochemical reactions, over-potentials and related electric parameters throughout the cell are calculated using the FLUENT add-on SOFC module.

2. Model Geometry

The geometry to be modeled in this paper is based on a tested anode-supported planar SOFC developed at the Chinese Academy of Science Ningbo Institute of Material Technology and Engineering (NIMTE). Figure 1 is the sketch of the SOFC structures for cross-flow configuration. The complete domain having 13 channels for fuel and air channels is adapted. Figure 2 displays the grid arrangement for the studied cell. The computational domain is divided into more than 2 million control volumes, all of which are high quality hexahedron meshes. The meshes are finer in the electrolyte, anode and cathode layers, and coarser for the air and fuel channels and for the interconnects. Grid independence

was achieved at 2.15×10^6 elements (Figure 2), after which the change in the maximum temperature was less than 1%, in maximum velocity less than 2%, in average current density less than 2%, in oxygen consumption less than 0.2% and in hydrogen consumption less than 1% (compared with the ones predicted by 3.00×10^6 elements). Table 1 shows the geometrical parameters of simulation domain.

Figure 1. Sketch of anode-supported planer SOFC structure for cross-flow configuration (not in scale).

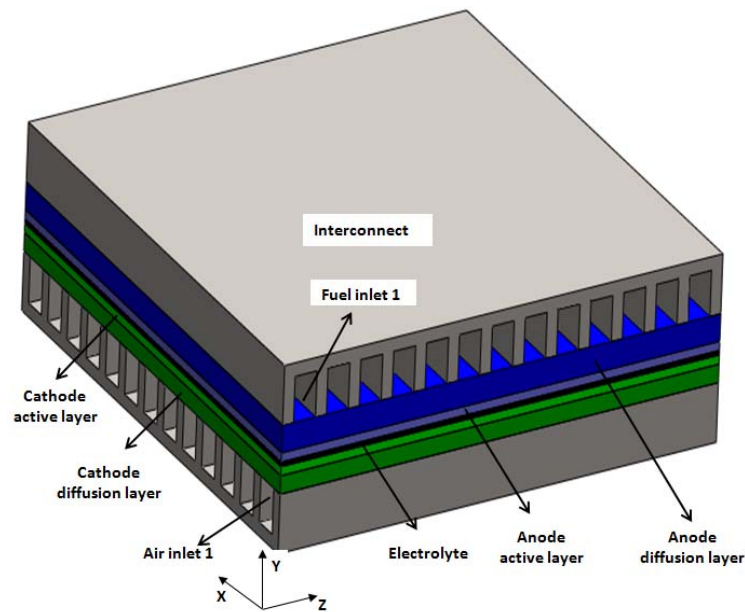


Figure 2. The mesh arrangement for the cross-flow configuration computation domain (not in scale).

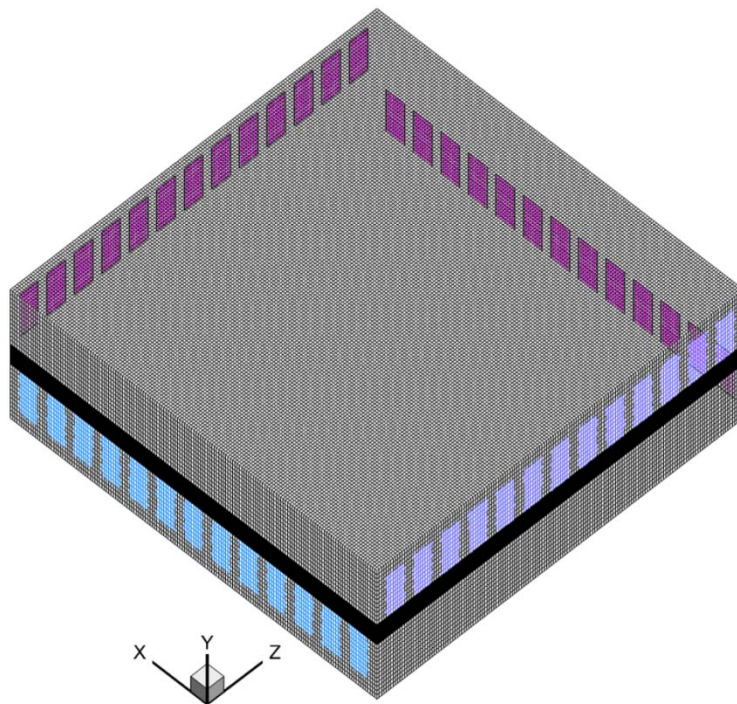


Table 1. Geometrical parameters of simulation domain.

Parameters	Values	Unit
Cell length (x-fuel, z-air)	40	mm
Cell width (z-fuel, x-air)	40	mm
Channel width (z-fuel, x-air)	2	mm
Channel height (y)	1	mm
Total number of channels	13	-
Thickness of the anode diffusion layer (y)	0.38	mm
Thickness of the anode/cathode active layer (y)	0.02	mm
Thickness of the cathode diffusion layer (y)	0.05	mm
Thickness of the electrolyte (y)	0.01	mm
Height of the interconnect (y)	1.3	mm

3. Mathematical Equations

Species transport in the porous electrodes occurs in the gas-phase, integrated with the electrochemical reactions at the solid active surfaces in the electrode active layers. The electrodes are porous and species transfer is dominated by gas diffusion [3]. The electrolyte has two functions: to transport oxygen ions from the cathode to the anode and to block electron and gas flow between the anode and cathode [4]. The flow of electrons (electronic charge) through external circuit balances the flow of ions (ionic charge) through the electrolyte when electrical power is produced [5]. The interconnect can be assumed to be impermeable to gases. Electron transport needs to be considered because the current from the SOFC is collected [6]. The governing equations to be solved are conservation of mass, momentum, charge, thermal energy and species. These transport equations are coupled with electrochemical processes through source/sink terms to describe the relevant processes in fuel cells.

3.1. Mass Continuity Equation

Equation (1) is used to describe the mass conservation for gas-phase components inside the cell and solved for the fuel and air channels and the respective electrodes:

$$\nabla(\rho_{\text{eff}}U) = S_m \quad (1)$$

where U represents the volume-averaged velocity vector of the species mixture; ρ_{eff} is the effective density of the mixture gases, to be evaluated as the mean values of different species:

$$\rho_{\text{eff}} = \sum_i X_i \times \rho_i \quad (2)$$

where X_i and ρ_i are the mass fraction and the density of the i th species, respectively.

The source term S_m in Equation (1) accounts for the mass balance caused by mass consumption or production from the electrochemical reaction (in catalyst layers or active layers).

It should be mentioned that the source terms can be expressed using the volumetric production/consumption rate of species due to the electrochemical reactions occurring at the

triple-phase boundary (TPB). For SOFCs, it corresponds to the hydrogen consumption and water generation on the anode side, oxygen consumption on the cathode side, respectively.

For the anode active layer:

$$S_m = (J_{H_2} + J_{H_2O}) \frac{A_{\text{active}}}{V} = \left(-\frac{I_{A,\text{act},a}}{2F} M_{H_2} + \frac{I_{A,\text{act},a}}{2F} M_{H_2O} \right) \frac{A_{\text{active}}}{V} \quad (3)$$

For the cathode active layer:

$$S_m = J_{O_2} \cdot \frac{A_{\text{active}}}{V} = -\frac{I_{A,\text{act},c}}{2F} M_{O_2} \cdot \frac{A_{\text{active}}}{V} \quad (4)$$

For the channels and diffusion layer: $S_m = 0$

In Equations (3) and (4), M_i means the molecular weight of the species, V refers to the volume of the control volume at the active sites, A_{active} the electrochemically active area per volume, F is Faraday's constant, $I_{A,\text{act},a/c}$ the volumetric transfer current of the reactions in the anode and cathode. We can define $A_{ve} = \frac{A_{\text{active}}}{V}$, to represent active surface area-to-volume ratio in TPB regions.

3.2. Momentum Conservation Equation

The governing equations for momentum transport is normally the Navier-Stokes equations applied in the fuel channels and the Darcy term added for the porous electrodes [7,8]. The physics of laminar and turbulent incompressible flow are well described by the Navier-Stokes equation, and it is a common practice to assume laminar flow for fuel cell gas channels due to the small velocities, which decreases the computational cost significantly [9].

The momentum equation reads:

$$\nabla(\rho_{\text{eff}}UU) = -\nabla P + \nabla(\mu_{\text{eff}}\nabla U) + S_d \quad (5)$$

where P is the pressure, for the mixture gases; μ_{eff} is the effective viscosity of the gas mixture:

$$\mu_{\text{eff}} = \sum_i Y_i \times \mu_i \quad (6)$$

where Y_i and μ_i are the mole fraction and viscosity of the i th species, respectively.

The source term S_d can be expressed as follows:

$$S_d = -\mu_{\text{eff}}U/\beta \quad (7)$$

where β is the porous layer permeability. This source term accounts for the linear relationship between the pressure gradient and flow rate by the Darcy law. It should be noted that Equation (7) is formulated to be generally valid for both the flow duct and the porous layers. The source term is zero in the flow duct, because the permeability β is infinite.

3.3. Heat Conservation Equation

The thermal energy equation can be expressed as:

$$\nabla(\rho_{\text{eff}}c_{p,\text{eff}}UT) = \nabla \left(k_{\text{eff}}\nabla T - \sum_i^n m_i h_i \right) + S_T \quad (8)$$

Equation (8) balances the convective energy, the heat conduction through the solid and the fuel gas mixture, the heat flux due to fuel gas species diffusion, and a source term S_T . h_i is the partial enthalpy of the i th species.

The effective parameters applied for the porous structures, such as effective thermal conductivity k_{eff} and effective specific heat $c_{p,eff}$, can be evaluated as:

$$k_{eff} = \varepsilon k_f + (1 - \varepsilon)k_s \quad (9)$$

$$c_{p,eff} = \varepsilon c_{p,f} + (1 - \varepsilon)c_{p,s} \quad (10)$$

where ε is the porosity; k_f and k_s are the thermal conductivities of the fluid and solid structure, respectively; $c_{p,f}$ and $c_{p,s}$ are the specific heat of the gas mixture and solid part of the porous material.

The source term for the thermal energy equation in the anode/cathode active layer due to the electrochemical reactions can be written as:

$$S_T = A_{ve} \times \left(R_e \Delta h_{ele} + I_{A,act,a/c} \times \eta_{act,a/c} + I_A^2 \times R_{ohm} \right) \quad (11)$$

The reaction rate of the electrochemical reaction, appearing in the source terms is:

$$R_e = \frac{I_{A,act,a/c}}{nF} \quad (12)$$

In Equation (11) Δh_{ele} is the net enthalpy change due to the electrochemical reactions, $I_{A,act,a/c} \times \eta_{act,a/c}$ is the product of the volumetric transfer current (A/m^3) and the activation over-potential in the anode or cathode active layer, the so-called three phase boundary (TPB), R_{ohm} is the ohmic resistivity in the charge conducting media. I_A (A/m^2) is the current flux density magnitude, n means number of electrons transferred per reaction.

3.4. The Species Conservation Equation

The species conservation equations are formulated in a general form:

$$\nabla(\rho_{eff} U Y_i) = \nabla(D_{i,eff} \nabla Y_i) + S_{g,i} \quad (13)$$

where Y_i is the mole fraction of the i th gas species; $D_{i,eff}$ represents the effective mass diffusion coefficient of the i th species; and $S_{g,i}$ the production/consumption rate of the i th species. The concentration of the inert species, nitrogen in the cathode, is determined from a summation of the mass fractions of the other species.

In the anode/cathode active layer:

$$S_{g,i} = A_{ve} \times R_e \times M_i \quad (14)$$

For the mass diffusion, the dusty-gas model is used in this work. The diffusion coefficients of species i in fuel duct are based on the binary coefficients, as given by [10,11]:

$$D_{i,gm} = \frac{1 - Y_i}{\sum_{i \neq j} \frac{Y_i}{D_{i,j}}} \quad (15)$$

where $D_{i,j}$ is the binary diffusion coefficients; and Y_i represents the mass fraction of the species i .

In the porous electrode, it is assumed that the mean free-path of the molecules is larger than the pore size which means the collisions between the molecules and the solid walls are more frequent than with other molecules. Then, Knudsen diffusion is evaluated as follows:

$$D_{i,k} = \frac{2}{3} r_e \times v_i = \frac{2}{3} r_e \sqrt{\frac{8RT}{\pi M_i}} \quad (16)$$

where r_e is the effective radius of the pores and v_i is the average molecular speed of species i . The effective diffusion coefficient can be expressed as: [11]

$$D_{i,eff} = \frac{\varepsilon D_{i,gm} \times D_{i,k}}{\tau D_{i,gm} + D_{i,k}} \quad (17)$$

where τ is tortuosity for characterization of fluid flow through the porous layer.

3.5. Ion and Electron Transport

The charge conservation equation is solved for the involved charge transport in the ionic/electronic phase. It involves the solution of the Poisson equations for the ionic/electric field over the entire region:

$$-\nabla(\sigma_{eff} \nabla \Phi) = S_\Phi \quad (18)$$

where σ_{eff} is effective ionic/electronic conductivity in the electrolyte or in the interconnects. The source term S_Φ is used to describe the transfer current between the electronic and electrolyte phases inside the anode and cathode active layers. Elsewhere in the gas flow ducts, diffusion layers, interconnects and electrolyte, S_Φ is zero, *i.e.*, the Poisson equation system reduces to the Laplacian equation.

The electronic conductivities ($\sigma_{electron}$) in the bulk anode (Ni) and the bulk cathode (LSM) materials, and ionic conductivity (σ_{ion}) in the bulk electrolyte material (8YSZ) are defined in Equations (19)–(21), respectively:

$$\sigma_{electron,a} = \frac{4.2 \times 10^7}{T} \exp\left(\frac{-1200}{T}\right) \quad (19)$$

$$\sigma_{electron,c} = \frac{9.5 \times 10^7}{T} \exp\left(\frac{-1150}{T}\right) \quad (20)$$

$$\sigma_{ion} = 3.34 \times 10^4 \times \exp\left(\frac{-10300}{T}\right) \quad (21)$$

For the porous electrodes, effective conductivity for electron/ion is estimated by Equation (22) [12]:

$$\sigma_{eff} = \left(\frac{1 - \varepsilon}{\tau}\right) \sigma \times V_{eff} \quad (22)$$

where ε means the porosity of the porous electrodes; τ is the tortuosity factor of charge transport and V_{eff} represents the volume fraction of Ni in the anode (or LSM in the cathode) and YSZ in the porous materials. Kanno *et al.* [13] calculated the tortuosity factors (by LBM) and the values between 7 and 17 are found for Ni and between 6 and 14 for YSZ, respectively. Iwai *et al.* [14] evaluated the tortuosity factors statistically with the random walk process of non-sorbing particles as well as with the LBM method, and values between 6.91 and 29.46 were found for Ni and between 9.84 and 27.89 for YSZ,

respectively, depending slightly on the evaluation methods, but mostly on the direction (x , y and z). The values used in this study are outlined in Table 2.

Table 2. Properties for the porous electrodes.

Domain	ε	τ	V_{eff}
Anode	0.3	10	YSZ:0.60/Ni:0.40
Cathode	0.3	10	YSZ:0.60/LSM:0.40

3.6. Electrochemical Reactions

In the anode duct, the fuel (e.g., H_2) is supplied and air ($\text{O}_2 + \text{N}_2$) is introduced in the cathode ducts. Reactants are transported by diffusion and/or convection to the TPBs, where electrochemical reactions take place.

The actual open-circuit voltage (OCV) varies locally with gas composition and temperature in the electrodes, which can be determined by the Nernst equation [Equation (23)] for the electrochemical reaction of pure hydrogen and oxygen.

$$OCV = E^0 - \frac{RT}{2F} \ln \left(\frac{P_{\text{H}_2\text{O}}}{P_{\text{H}_2} \sqrt{P_{\text{O}_2}}} \right) \quad (23)$$

where p_{H_2} , p_{O_2} , $p_{\text{H}_2\text{O}}$ represent the partial pressures of hydrogen, oxygen, and water vapor, respectively; R is gas constant; E^0 stands for the potential for the hydrogen oxidation reaction at the standard temperature and pressure, which is evaluated by the change of Gibbs free energy $\Delta_f g$ for the formation reaction of water divided by $2F$, as shown in Equation (24):

$$E^0 = \frac{\Delta_f g}{2F} \quad (24)$$

The open-circuit potential (OCV) is the maximum voltage which can be achieved by a fuel cell when no current flow is applied. However, the actual voltage of a real cell (E), *i.e.*, the potential difference between the cathode and the anode, is lower than OCV when a current flow is applied. The difference between OCV and cell voltage E is due to the various potential losses. For the current work, the ohmic losses in the solid part of the SOFC, and activation and concentration losses at the TPBs are considered. Therefore, the operating cell voltage (E) can be expressed by Equation (25):

$$E = OCV - \eta_{\text{act},a/c} - \eta_{\text{conc},a/c} - I \times R_{\text{ohm}} \quad (25)$$

where I is the local current density; the second to the forth terms on the right hand side of Equation (25) express the activation and concentration losses at the electrode active layers; and the ohmic losses due to the current flow, respectively. The concentration losses occur when the mass transport rate to the reacting sites is too slow to supply the required amount of reactants for the reactions. This happens particularly at high current densities, when the reactions rate is high.

The activation loss (or over-potential) represents the energy lost due to the slowness of electrochemical reactions at the anode and the cathode active layers. A potential difference is needed at the interfaces between the electrode (metal for the electrons) and electrolyte material (YSZ for the ions) to drive the reaction away from equilibrium. In the equilibrium, the forward and backward reactions are happening at an equal rate. There are two activation over-potentials: one for the anode

active layer and one for the cathode active layer. For each of these over-potentials, the Butler-Volmer equation relates the local value to the current density, as below:

$$I_A = i_0 \left(\frac{[A]}{[A_{\text{ref}}]} \right)^\gamma \left[\exp \left(\frac{\alpha n F \eta_{\text{act,an}}}{RT} \right) - \exp \left(- \frac{(1 - \alpha) n F \eta_{\text{act,an}}}{RT} \right) \right] \quad (26)$$

$$I_C = i_0 \left(\frac{[C]}{[C_{\text{ref}}]} \right)^\gamma \left[\exp \left(\frac{\alpha n F \eta_{\text{act,cat}}}{RT} \right) - \exp \left(- \frac{(1 - \alpha) n F \eta_{\text{act,cat}}}{RT} \right) \right] \quad (27)$$

where i_0 = reference exchange current density per active surface area (A/m^2); $[A]$ and $[A]_{\text{ref}}$ = H_2 concentration and its reference value (mol/m^3); $[C]$ and $[C]_{\text{ref}}$ = O_2 concentration and its reference value (mol/m^3); γ = concentration dependence; α = transfer coefficient (dimensionless); F = Faraday constant ($9.65 \times 10^7 \text{ C/mol}$); i_0 can be expressed by Equation (28), and Table 3 shows the reference parameters applied for the exchange current density, where A_i is pre-exponential factor; E_a is the activation energy:

$$i_0 = \frac{RT}{nF} A_i \times \exp \left(- \frac{E_a}{RT} \right) \quad (28)$$

Table 3. Reference parameters for electrochemical reactions [15,16].

Domain	$[-]_{\text{ref}} \text{ mol/m}^3$	r	α	$A_i \text{ 1/}(\Omega\text{m}^2)$	$E_a \text{ (kJ/mol)}$	n
Anode	10.78	0.5	0.5	6.54×10^{11}	140	2
Cathode	2.38	0.5	0.5	2.35×10^{11}	137	2

4. Input Parameters and Boundary Conditions

The operating conditions and input parameters for the developed model are listed in Tables 4 and 5. The potential at the anode current collector is set to zero and the one at the cathode current collector as the cell operating voltage (0.7 V in this study). All other external boundaries and interfaces are electrically insulated.

Table 4. Properties for different components of the cell.

Title	Anode diffusion layer	Anode active layer	Electrolyte	Cathode active layer	Cathode diffusion layer	Solid interconnect
Porosity [17] ε	0.3	0.3	0	0.3	0.3	0
Permeability $\beta \text{ (m}^2\text{)}$	2×10^{-10}	2×10^{-11}	0	2×10^{-11}	2×10^{-10}	0
Specific heat [18] $C_p \text{ (J/kg K)}$	450	450	550	430	430	550
Thermal conductivity [6] $K \text{ (W/m}\cdot\text{K)}$	11	11	2.7	6	6	20
Active surface area to volume ratio, $A_{\text{ve}}, \text{ (m}^2\text{/m}^3\text{)}$	1.08×10^5	1.3×10^5	-	1.3×10^5	1.08×10^5	-

Table 5. Major boundary conditions of SOFC model.

Title	Boundary condition	Temperature, K	Species	Oxygen ion	Electron
Fuel inlet per duct	Mass flow rate: 2×10^{-8} kg/s	$T = 1073$	$Y_{H_2} = 0.95$ $Y_{H_2O} = 0.05$	None	None
Top wall of the anode interconnect	Wall	Adiabatic	None	None	0 V
Bottom wall of the cathode interconnect	Wall	Adiabatic	None	None	0.7 V
Air inlet per duct	Mass flow rate: 8×10^{-7} kg/s	$T = 1073$	$Y_{O_2} = 0.233$ $Y_{N_2} = 0.767$	None	None
Fuel outlet	Pressure outlet	convection	convection	None	None
Air outlet	Pressure outlet	convection	convection	None	None

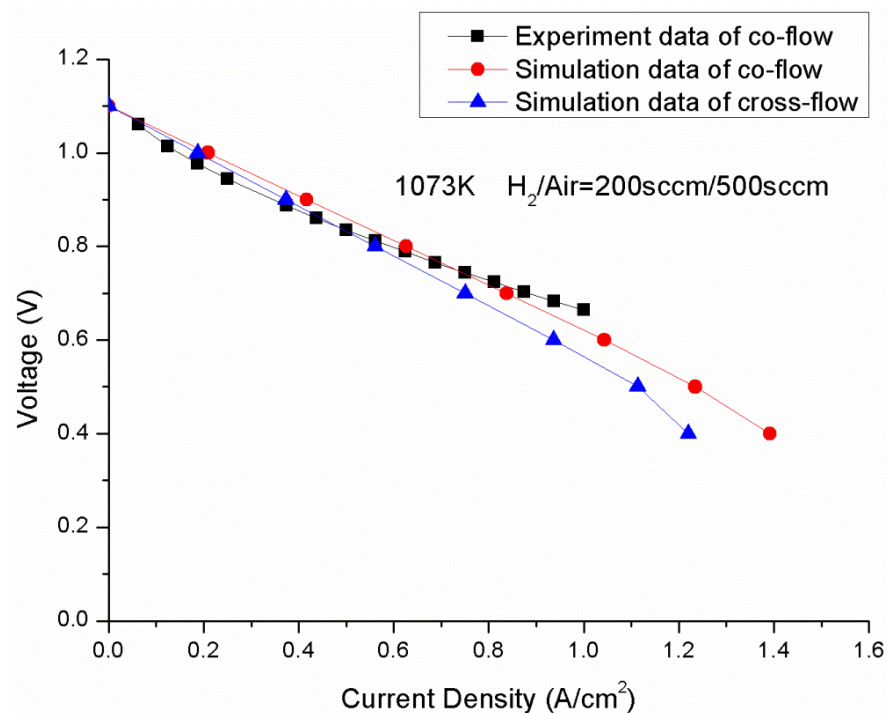
5. Simulation Results and Discussion

The SOFC model outlined above is implemented by using the finite volume method (FVM) in the commercial code Ansys/Fluent 14, with the add-on fuel cell module. The SIMPLE scheme is used to calculate the velocity coupling with pressure, and the second order upwind differencing scheme (UDS) is used for convection and diffusion coupling. The user-defined function (UDF) file is compiled into the model to define the electrochemical reactions and the source terms for the governing equations.

Ni-YSZ anode-supported SOFCs developed at the Chinese Academy of Sciences NIMTE were used for both the modeling and the experiment. The dimensions of the cells are $4 \times 4 \text{ cm}^2$, in which, a 400 μm thick Ni/8YSZ anode substrate was prepared by tape casting, followed by a 20 μm thick anode functional layer (anode TPB layer) and a 10 μm thick 8YSZ electrolyte layer. The cathode of the cell is a double LSM layer sprayed onto the anode substrate before it was co-sintered. The cells were tested in an alumina testing chamber. Platinum and nickel foils were used as current collectors at the cathode and anode sides, respectively. Silver mesh sandwiched between LSM was utilized for gas distribution at the cathode side; the silver mesh was applied to decrease the contact resistance between the cathode and the current collector. For the anode side, two layers of nickel foam were used for gas distribution and current collection. Air and humidified hydrogen were introduced into the cathode and anode, respectively. The operating temperature was 800 °C. The flow rate of hydrogen was 200 sccm, and the air flow rate was 500 sccm. Figure 3 shows the V-I curve predicted from CFD model compared with the experimental data under the same operating conditions. The cell was tested in a 800 °C heated oven, so the thermal isolation is assumed for the external walls during the validation, to agree with the experimental conditions.

Considering the cells in the stack (except the cell at the top and bottom), we can define the outside wall of the cell being adiabatic. The operating conditions for the developed model are given as follows: operating voltage 0.7 V; the mass flow rate of fuel inlet per duct: 2×10^{-8} kg/s, the mass flow rate of air inlet per duct: 0.8×10^{-6} kg/s, as specified in Table 5.

Figure 3. Comparison of the predicted V - I curve from CFD model with experimental data at the same operating condition.



6.1. Temperature Distribution

The predicted temperature distribution in the cell is shown in Figure 4. It is found in the Figure 4a that the temperature in the anode and cathode inlet is the lowest (1073 K), then it rises along the flow directions as the heat is generated due to the electrochemical reactions. The temperature reaches the maximum value about 1150 K in the regions close to the outlets of the fuel and air channels. Figure 4b shows the temperature distribution along the cell thickness direction (y) in the plane $z = 0.02$ m. The temperature in the air channels (bottom part) is lower than that in fuel channel at the same x position. This is because the mass flow rate of air (500 sccm) in the cathode is substantially higher than that in the anode side (200 sccm), and more heat is taken away by the flowing air.

Figure 5 shows the temperature distribution along the fuel main flow direction in the plane $z = 0.02$ m at different cell height, *i.e.*, $y = 0.0011$ m, 0.00138 m and 0.0022 m, respectively. It is revealed that, for the cross-flow arrangement, the temperature difference between different cell heights is very small and the temperatures in the fuel channel ($y = 0.0022$ m) and the electrolyte ($y = 0.00138$ m) are all increased along the fuel flow direction (x -direction), and the value of the temperature for $y = 0.0011$ m is a wave-shaped curve. This is because the temperature of the air is lower than that of the solid part in the cathode (see Figure 4b); The temperature in the electrolyte is the highest because of the heat source produced by the electrochemical reactions occurring nearby.

Figure 4. Temperature (K) distribution (not in scale): (a) inside the cell; (b) in the plane ($z = 0.02$ m).

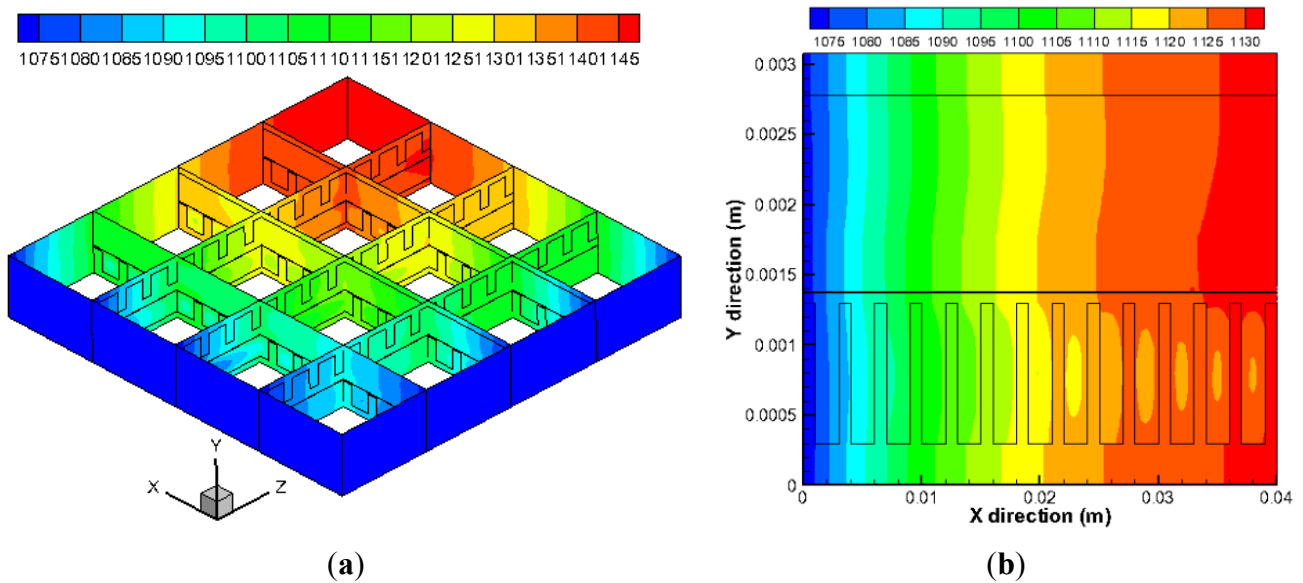
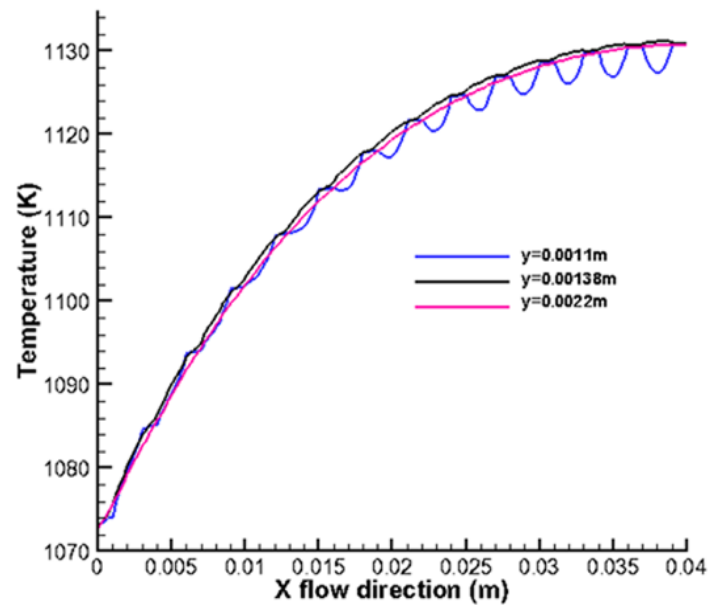


Figure 5. Temperature (K) distribution along the fuel main flow direction in the plane ($z = 0.02$ m) at positions of $y = 0.0011$ m, 0.00138 m and 0.0022 m for cross-flow.



6.2 Flow Field of Gases

Figure 6 shows the predicted velocity distribution in both the anode and cathode. As shown in Figure 6, the velocity in the air channel is much larger than that in the fuel channel. This is because the gas flow rate in the cathode (500 sccm) is substantially higher than that in the anode side (200 sccm).

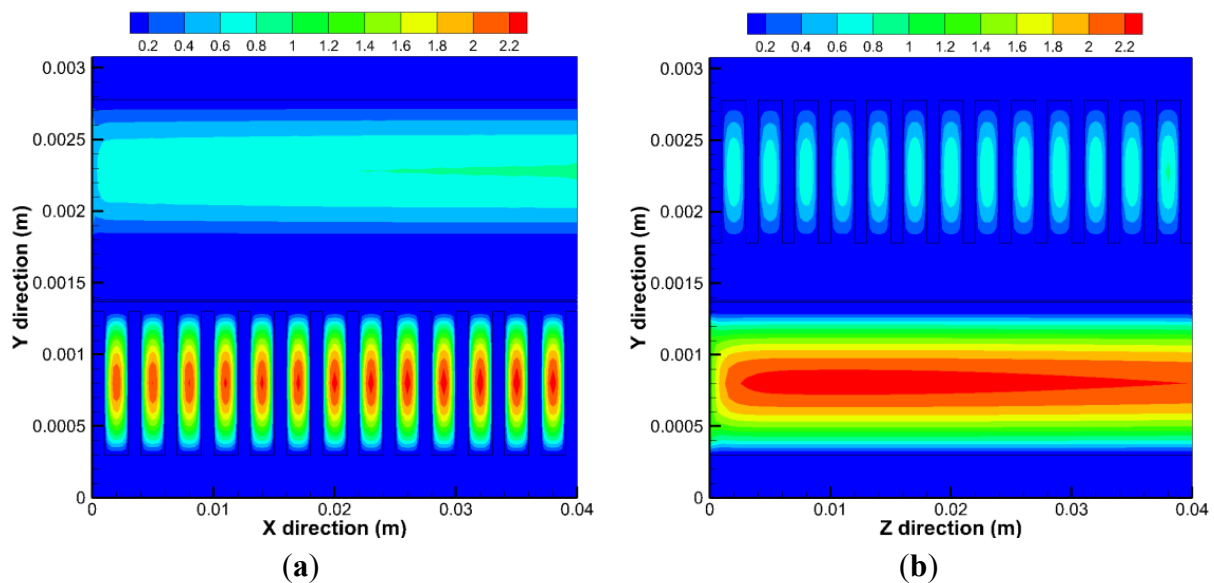
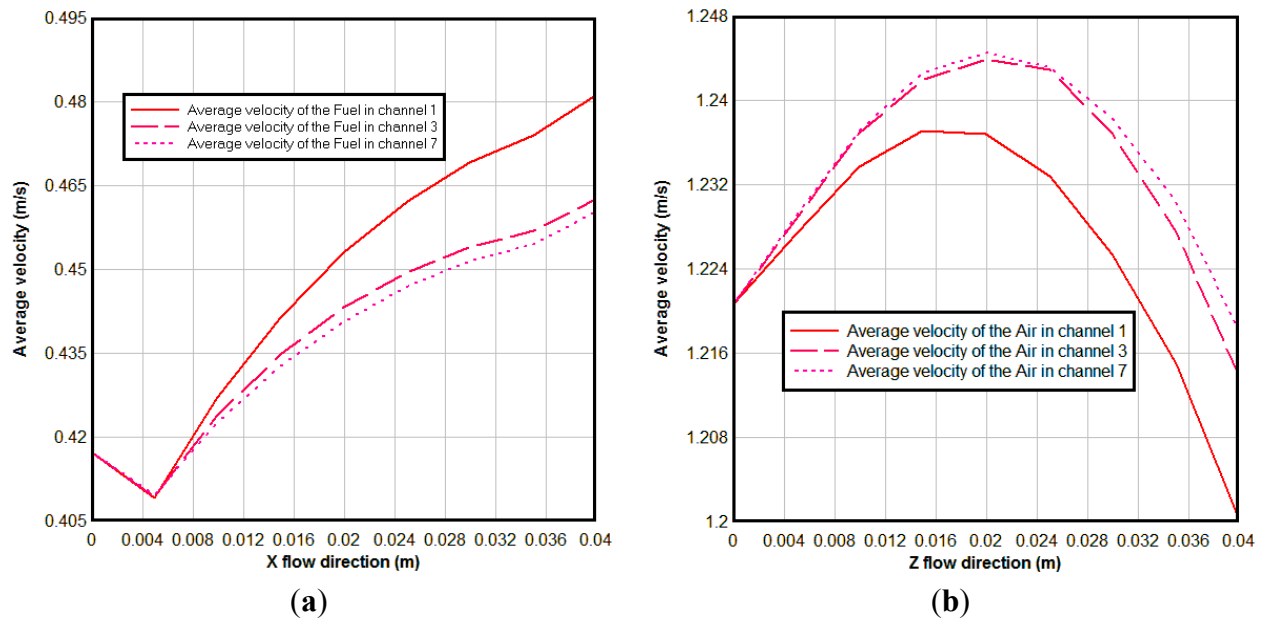
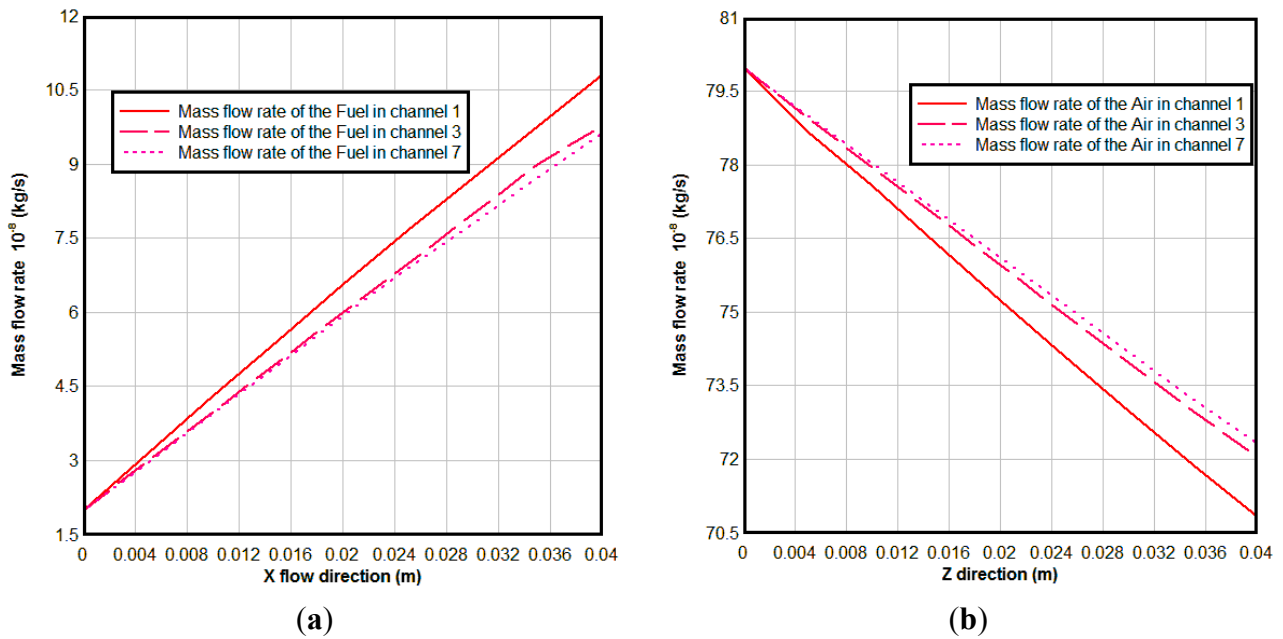
Figure 6. Velocity of the gas in different plane (not in scale): (a) $y = 0.02$ m; (b) $x = 0.02$ m.

Figure 7 shows the average velocity of the gas in different channels. From Figure 7a we can see the average velocity of the fuel is decreased at first from the channel inlet, due to the fuel diffused to the anode diffusion layer at the beginning; then it is increased along the flow direction, it is so because the temperature is increased along the main flow direction and H_2O generation due to the electrochemical reactions in the anodic TPBs. It can be seen also that the average velocity in the channel 1 is bigger than that in channel 3 and 7. This happened due to two reasons: first, the channel 1 is at the side of the cell, and correspondingly more reaction areas are expected; second, channel 1 is near the air inlet where the concentration of the O_2 is higher. More reaction areas and high concentration of the O_2 result in stronger electrochemical reactions here. At the cathode the oxidant reduction reaction occurs, *i.e.*, O_2 is consumed. This may reduce the velocity of the air in the air channel. At the same time, the high temperature increases the velocity of the air. In overall, the air velocity magnitude reaches to a maximum value and then decreases to the lowest value in the outlet, as seen in Figure 7b. The same reasons as for in the anode cause the average velocity of air channel 1 being lower than that in channels 3 and 7.

Figure 8 is the mass flow rate of the gases in different channels, From Figure 8, we can see that the mass flow rate of the fuel increases along the fuel flow direction, because of the H_2O generation due to the electrochemical reactions in the anodic TPBs; while the mass flow rate of the air decreases along the air flow direction due to the O_2 consumed in the cathode. The reason for the mass flow rate of fuel in channel 1 being bigger than that in channel 3 and channel 7 is that more reaction areas and high concentration of the O_2 result in stronger electrochemical reactions here.

From Figures 7 and 8, we can see that although there is a constant mass flow rate of gas in the inlet of each channel, the flow distribution is non-uniform along the flow direction because electrochemical reaction rate is different in different locations. The amount of fuel transported to the active surfaces for the electrochemical reactions is governed by different parameters, such as porous microstructure, gas consumption rate, pressure gradient between the fuel flow duct and the porous anode, and the inlet conditions, *etc.* [19].

Figure 7. Average velocity of the gas in: (a) fuel; (b) air channels.**Figure 8.** Mass flow rate of the gas in: (a) fuel; (b) air channels.

6.3 Mole Fraction of the Gases

For the case of H_2/H_2O composition of 0.95/0.05, air as oxidant, 800 °C and cell operating voltage 0.7 V, the mole fractions of hydrogen at the inlet and outlet are 0.95 and 0.4, respectively. Based on Equation (29), the fuel utilization is about 0.60:

$$U_f = \frac{y_{H_2, \text{inlet}} - y_{H_2, \text{outlet}}}{y_{H_2, \text{inlet}}} \quad (29)$$

From Equation (23), the mole fraction or partial pressure of hydrogen in the anode is an important factor determining *OCV* and thus the current density. In the anode channels, the mole fraction of

hydrogen is high, which diffuses towards the active layer, for the electrochemical reaction. Hydrogen is consumed and water vapor generated. It is also interesting to have a close look at the hydrogen distribution inside the anode and fuel channels.

Figure 9 shows the mole fraction distribution of gases for a cross-flow section in the plane $x = 0.03$ m. In Figure 9a, the bottom (y is 0.00137–0.00138 m) and top (y is 0.00278–0.00308 m) regions represent the electrolyte and interconnect, respectively, while the middle parts are for fuel channels/ribs (y is 0.00178–0.00278 m) and anode (y is 0.00138–0.00178 m). It is clear that the mole fraction of H_2 in the side channels is smaller compared with the middle channels. It can be also seen that the mole fraction of H_2 decreases in the electrode from the fuel channel/electrode interface ($y = 0.00178$ m) to electrode/electrolyte interface ($y = 0.00138$ m), while the opposite finding is observed for H_2O in Figure 9b. This is due to the electrochemical reaction occurring at the bottom of the anode, where there is a depletion of hydrogen and production of water vapor. The gradients are higher in the porous zone because the fluid flow velocity is much smaller in the substrate of the anode. The H_2 mass transport by the diffusion becomes dominant compared to the convective mass transport. It is also found that, due to H_2 mole fractions unevenly distributed between each channels, a very small mole fraction of H_2 appears in the anode under the side channels. For the porous region under the channels, it is revealed that the mole fraction of H_2 is higher, while for the regions under the ribs between the channels, the mole fraction is lower. It is so because the H_2 diffusion to the places under the ribs is much limited due to the longer diffusion pathway.

Figure 9. Mole fraction for a cross-section in the plane $x = 0.03$ m for: (a) H_2 ; (b) H_2O (not in scale).

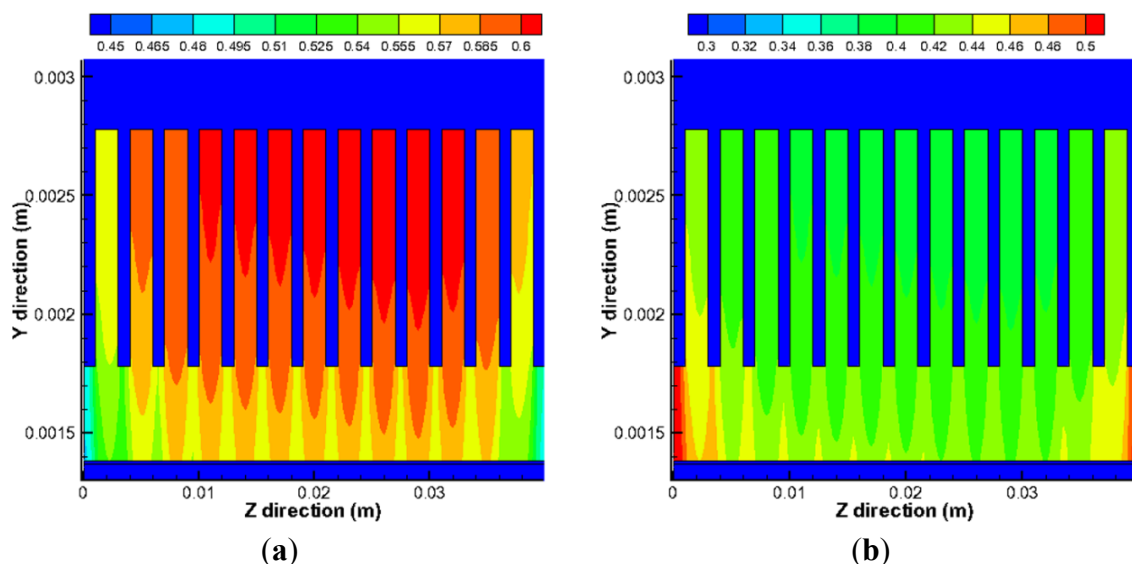
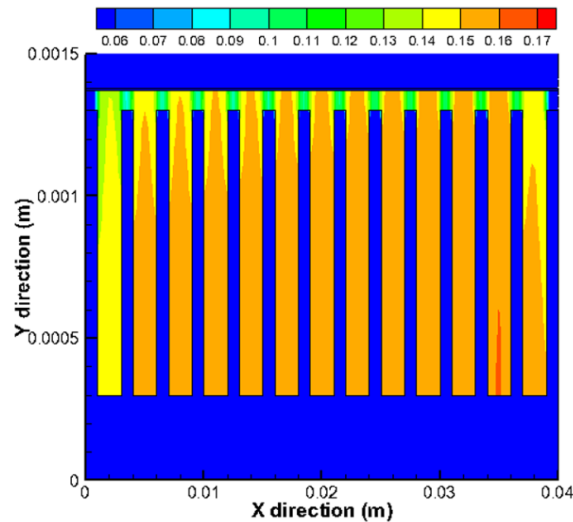


Figure 10 is the mole fraction of O_2 for a cross-section in the plane $z = 0.03$ m. In Figure 10, the bottom (y is 0–0.0003 m) and top (y is 0.00137–0.00138 m) regions represent the interconnect and electrolyte, respectively, while the middle parts are for channels/ribs (y is 0.0003–0.0013 m) and cathode (y is 0.0013–0.00137 m). It is found that the O_2 has almost the similar distribution as the H_2 (Figure 9a), except that the mole fraction of the O_2 in the cathode electrode/electrolyte interface ($y = 0.00137$ m) is higher than that of the H_2 . This is because the cathode (0.07 mm) is much thinner than the anode (0.4 mm). On the other hand, the O_2 is hardly diffused to the places under the ribs

compared with those under the channels in such a thin thickness, which results in a stepped distribution of O_2 in the cathode (y is 0.0013–0.00137 m).

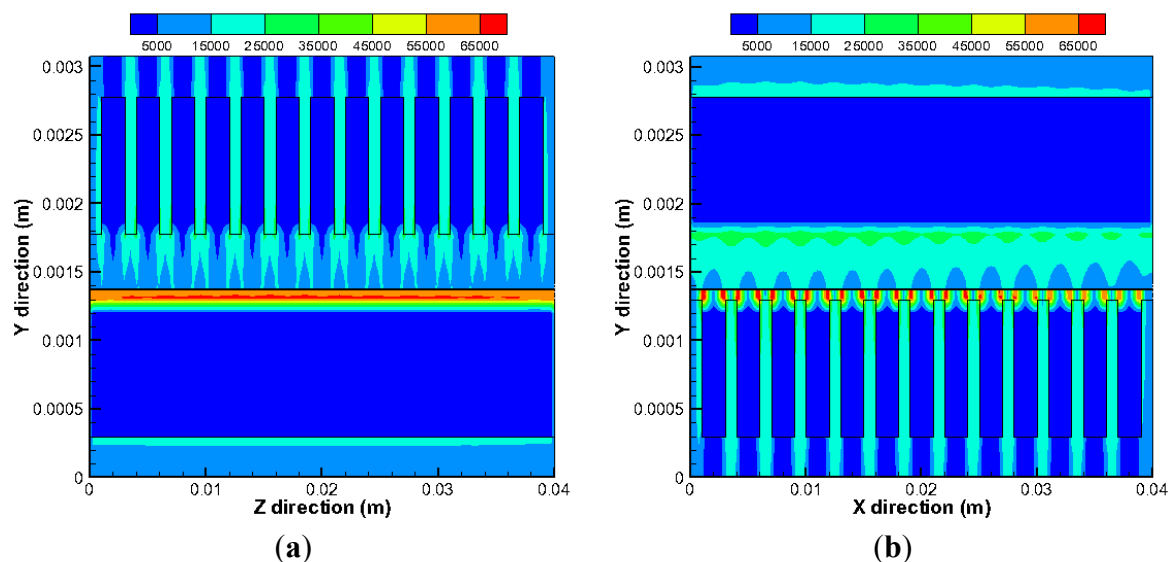
Figure 10. Mole fraction of O_2 for a cross-section in the plane $z = 0.03$ m (not in scale).



6.4. Current Density Distribution

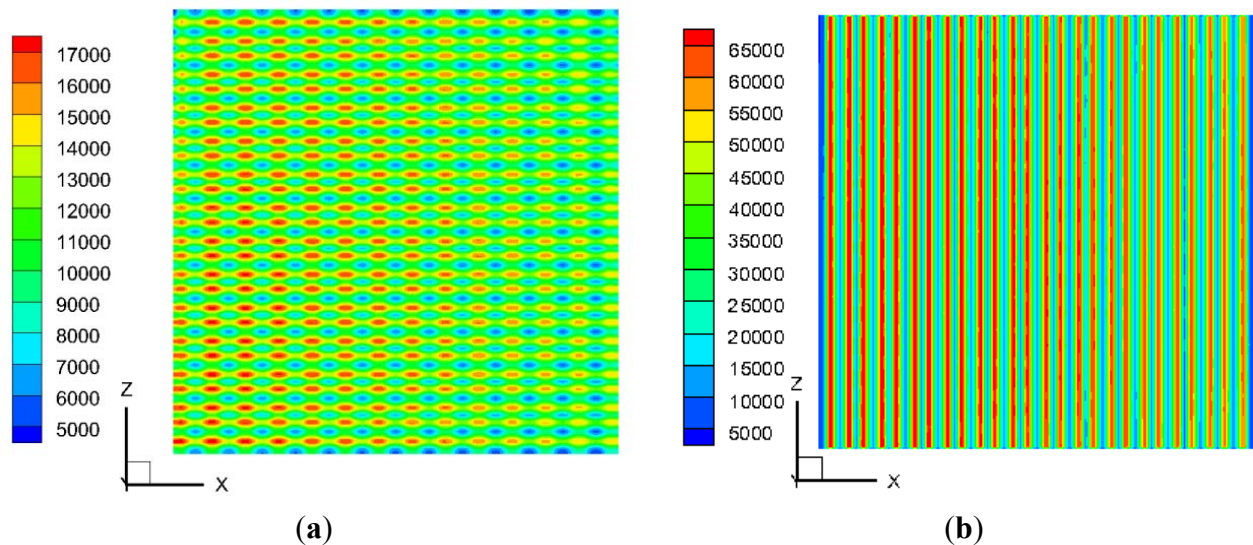
From Figure 11a, it is revealed that the current density distribution along the air main flow direction is very uneven in the electrodes, and the maximum value is located at the interfaces between the ribs and the cathode electrodes, and the minimum value appears in the anode electrodes corresponding to the middle of the channels. This is so because the electrons always transfer in the shortest path. From Figure 11b, it is also found that the maximum value of the current density in the cathode is decreased along the X direction as the hydrogen in the fuel is being consumed along this direction and its concentration decreases.

Figure 11. Current density (A/m^2) distribution for a cross-section in the plane for: (a) $x = 0.03$ m; (b) $z = 0.03$ m (not in scale).



From Figure 12, we can find that the maximum current density in the cathode active area is larger than that in anode active area. The reason is that the thickness of the cathode electrode (0.07 mm) is much smaller than that of the anode (0.4 mm). It is also seen that the current density is decreased along the fuel flow direction (X direction), as the fuel concentration becomes low, even compensated by an increased temperature along the main flow direction [20].

Figure 12. Current density (A/m^2) distribution in the active area of the cell for: (a) anodic active area ($y = 0.001385$ m), and (b) cathodic active area ($y = 0.00137$ m).



Generally speaking, the distribution of the current density is determined by various parameters, such as porous microstructure, gas concentration, geometry structure of the gas channel, operating conditions. A big current density results in a big over-potential in the active area, and also leads to the big ohmic heat generation ($I_A^2 \times R_{ohm}$) there. The uneven current density distribution is harmful to the performance and working life time of the fuel cells.

7. Conclusions

In this study, a three-dimensional computational fluid dynamics (CFD) model has been developed and applied for an anode-supported planar SOFC. The simulation results of the developed model are in agreement with the experimental data obtained under the same conditions. With the simulation results, the distribution of temperature, flow velocity and the fuel gas concentrations through the cell components and gas channels are presented and discussed. Potential and current density distributions in the cell and overall fuel utilization are also presented. It is found that the significant temperature gradients exist along the length of the cell, and the maximum value of the temperature for the cross-flow is at the outlet region of the cell. The distribution of the current density is uneven, and the maximum of the current density is located at the interfaces between the channels, ribs and the electrodes. The maximum current density results in the large over-potential and heat source in the electrodes, which is harmful to the overall performance and working life time of the fuel cells. New types of flow structures may be possible to make the current flow more evenly distributed and promote most of the TPB areas taking part in the electrochemical reaction.

Acknowledgments

This work was supported by the National Natural Science Foundation of China (21276036).

Conflicts of Interest

The authors declare no conflict of interest.

References

1. Li, P.-W.; Schaefer, L.; Chyu, M.K. Transport Phenomena in Fuel Cells. In *Multiple Transport Processes in Solid Oxide Fuel Cells*; ISBN 9781853128400; Sundén, B., Faghri, M., Eds.; WIT Press: Southampton, UK, 2005; Chapter 1.
2. Yuan, J.; Huang, Y.; Sundén, B.; Wang, W.G. Analysis of parameter effects on chemical reaction coupled transport phenomena in SOFC anodes. *Heat Mass Transf.* **2009**, *45*, 471–484.
3. Nam, J.H.; Jeon, D.H. A comprehensive micro-scale model for transport and reaction in intermediate temperature solid oxide fuel cells. *Electrochim. Acta* **2006**, *51*, 3446–3460.
4. Goodenough, J.B.; Huang, Y.-H. Alternative anode materials for solid oxide fuel cells. *J. Power Sources* **2007**, *173*, 1–10.
5. Haile, S.M. Fuel cell materials and components. *Acta Mater.* **2003**, *51*, 1981–2000.
6. Kakac, S.; Pramuanjaroenkij, A.; Zhou, X.Y. A review of numerical modeling of solid oxide fuel cells. *Int. J. Hydrog. Energy* **2007**, *32*, 761–786.
7. Versteeg, H.K.; Malalasekera, W. *An Introduction to Computational Fluid Dynamics: The Finite Volume Method*; Pearson: London, UK, 1995.
8. Damm, D.L.; Fedorov, A.G. Local thermal non-equilibrium effects in porous electrodes of the hydrogen fueled SOFC. *J. Power Sources* **2006**, *159*, 1153–1157.
9. Chao, C.H.; Hwang, A.J.J. Predictions of phase temperatures in a porous cathode of polymer electrolyte fuel cells using a two-equation model. *J. Power Sources* **2006**, *160*, 1122–1130.
10. Yuan, J.; Faghri, M.; Sundén, B. Chapter 4: On Heat and Mass Transfer Phenomena in PEMFC and SOFC and Modeling Approaches. In *Transport Phenomena in Fuel Cells*; ISBN 1-85312-840-6; Sundén, B., Faghri, M., Eds.; WIT Press: Ashurst Lodge, Ashurst Southampton, UK, 2005; pp. 133–174.
11. Yuan, J.; Sundén, B. On mechanisms and models of multi-component gas diffusion in porous structures of fuel cell electrodes. *Int. J. Heat Mass Transf.* **2014**, *69*, 358–374.
12. Hussain, M.M.; Li, X.; Dincer, I. Mathematical modeling of transport phenomena in porous SOFC anodes. *Int. J. Therm. Sci.* **2007**, *46*, 48–56.
13. Kanno, D.; Shikazono, N.; Takagi, N.; Matsuzaki, K.; Kasagi, N. Evaluation of SOFC anode polarization simulation using three-dimensional microstructures reconstructed by FIB tomography. *Electrochim. Acta* **2011**, *56*, 4015–4021.
14. Iwai, H.; Shikazono, N.; Matsui, T.; Teshima, H.; Kishimoto, M.; Kishida, R.; Hayashi, D.; Matsuzaki, K.; Kanno, D.; Saito, M.; *et al.* Quantification of SOFC anode microstructure based on dual beam FIB-SEM technique. *J. Power Sources* **2010**, *195*, 955–961.

15. Aguiar, P.; Adjiman, C.S.; Brandon, N.P. Anode-supported intermediate temperature direct internal reforming solid oxide fuel cell. I: Model-based steady-state performance. *J. Power Sources* **2004**, *138*, 120–136.
16. Patcharavorachor, Y.; Arpornwichanop, A.; Chuachuebsuk, A. Electrochemical study of a planar solid oxide fuel cell: Role of support structures. *J. Power Sources* **2001**, *93*, 130–140.
17. Andersson, M.; Yuan, J.; Sundén, B. SOFC modeling considering electrochemical reactions at the active three phase boundaries. *Int. J. Heat Mass Transfer* **2012**, *55*, 773–788.
18. Janardhanan, V.; Deutschmann, O. CFD analysis of a solid oxide fuel cell with internal reforming: Coupled interactions of transport, heterogeneous catalysis and electrochemical processes, *J. Power Sources* **2006**, *162*, 1192–1202.
19. Yuan, J.; Sundén, B. Analysis of chemically reacting transport phenomena in an anode duct of intermediate temperature SOFCs. *ASME J. Fuel Cell Sci. Technol.* **2006**, *3*, 89–98.
20. Zhu, H.; Kee, R.J.; Janardhanan, V.M.; Deutschmann, O.; Goodwin, D.G. Modeling elementary heterogeneous chemistry and electrochemistry in solid-oxide fuel cells. *J. Electrochem. Soc.* **2005**, *152*, A2427–A2440.

© 2013 by the authors; licensee MDPI, Basel, Switzerland. This article is an open access article distributed under the terms and conditions of the Creative Commons Attribution license (<http://creativecommons.org/licenses/by/3.0/>).